STM characterization of extended dislocation configurations in Au(001)

J. de la Figuera, M. A. González, R. García-Martínez, and J. M. Rojo
Departamento de Física de Materiales, Universidad Complutense, 28040 Madrid, Spain

O. S. Hernán, A. L. Vázquez de Parga, and R. Miranda
Departamento de Física de la Materia Condensada, Universidad Autónoma, Cantoblanco, 28049 Madrid, Spain

(Received 16 October 1997)

Scanning tunneling microscopy (STM) of Au(001) single crystals has been used to characterize dislocation configurations resulting mainly from nanoindentation of the surface by contact with the STM tip. The Burgers vectors and directions of the different extended dislocations are identified by comparing STM pictures with simulated images of the corresponding atomic configurations. We describe a configuration consisting of an unfaulted dislocation loop split into two pairs of Shockley partials, linked by a stair-rod segment that holds the two stacking-fault ribbons. The separation between Shockley partials in the extended dislocations is found to be larger than in the bulk. [S0163-1829(98)04527-5]

Crystal dislocations are often assumed to play a substantial role in a number of surface-related phenomena. Among others, dislocations control the growth rate of crystals from the vapor or from solution and accelerate its etching by chemical reagents.[1] They are also believed to govern the strain relaxation in heteroepitaxial growth,[2] to provide local points of enhanced surface reactivity[3] or alternate paths for diffusion of islands,[4] and to form complex networks underlying certain surface reconstructions.[5] Conversely, the state of the surface is suspected to influence the generation and motion of dislocations, which, in turn, control the mechanical properties of solids.[6] Whereas dislocations in the bulk of crystals are well described in textbooks[7] and ample experimental evidence of their most important properties has been accreted, particularly by means of transmission electron microscopy[8] (TEM), a systematic description of the properties of dislocations in relation to surfaces is still lacking. With the advent of scanning tunneling microscopy (STM) several recent studies have reported detailed imaging of dislocations in surfaces.[9] However, a comprehensive analysis of these images in terms of current dislocation theory has been seldom attempted.[10] This is a serious hindrance in current active fields, such as surface reconstruction[5] or surface radiation damage.[11]

In this paper, we report results of a STM study of a number of dislocation configurations in Au(001) surfaces, customarily found in the neighborhood of the contact point of the STM tip with the crystal. We identify their Burgers vectors and segment orientation, including dislocations with Burgers vectors parallel to the surface. This is done by comparing the STM images with those simulated by a simple model that combines dislocation theory with a hard-sphere model based in the atomic-charge superposition approximation.[12] We find split dislocations whose equilibrium distances are larger than expected from their bulk behavior. In addition, another type of surface defect is identified: it arises from dislocation *loop* splitting and consists of two stacking-fault ribbons, limited by Shockley partials, and sustained by a stair-rod dislocation segment. Splitting an originally unfaulted loop near the surface can have important consequences in regard to thin-film growth and related processes, not the least because unfaulted loops, with Burgers vector parallel to the surface, do not give rise to surface steps whereas a split configuration does.

The experiments were carried out at room temperature with a homemade STM operating in a vacuum in the range of 10^{-10} mbar. Gold single crystals with (001) orientation were cleaned by standard procedures including diamond-paste mechanical polishing (down to 0.25 μm) followed by argon-ion bombardment (600 eV) and 900 K annealing in ultrahigh vacuum. After several cycles, the sample appeared free of contaminants, as detected by Auger spectroscopy, and consisted of wide terraces with a typical width of 500 Å. In Fig. 1, we show an atomic resolution picture of the characteristic $5\times n$ reconstruction. As is well known, the value of n is sensitive to defect concentration, stresses,[13] etc. In our samples, typically $n=23\pm 2$. The defects we report in this paper were mostly observed in the neighborhood of the points of mechanical contact of the STM tungsten tip with the crystal, but similar defects were also found (less frequently) in other parts of the surface. The tip-sample con-

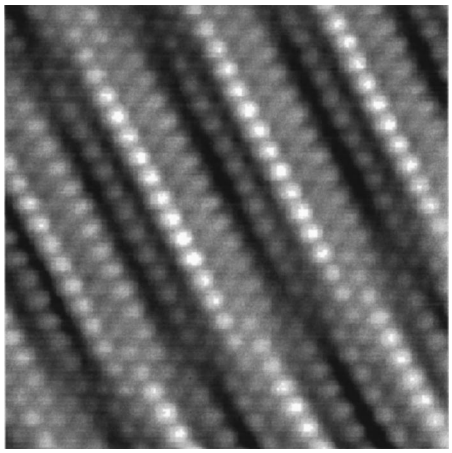

FIG. 1. High-resolution image of the reconstructed Au(100) surface showing the two periods of the reconstruction. The image frame is 53×53 Å.

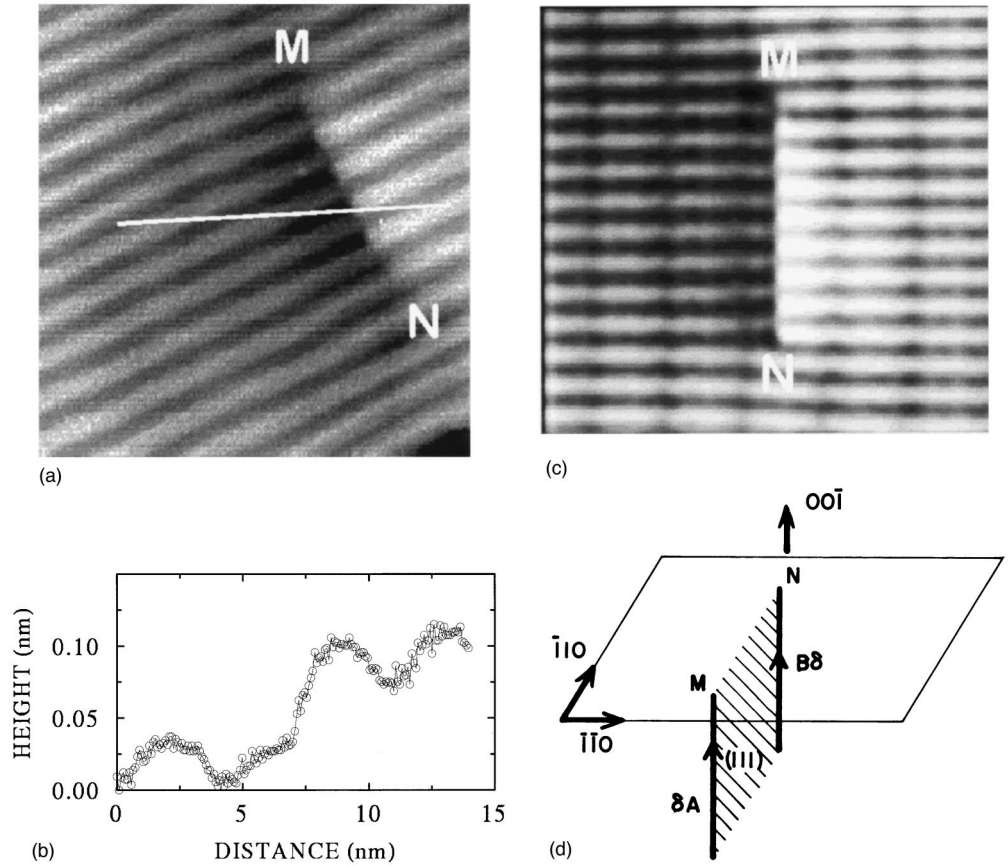

FIG. 2. (a) STM image of a type-I defect (extended perfect dislocation), with associated step *perpendicular* to the reconstruction. The image frame is 165×175 Å. (b) Profile along the solid line shown in image (a). (c) Simulated image of the dislocation configuration schematically described in (d). (d) Proposed final configuration: two parallel Shockley partials with Burgers vectors $\delta\mathbf{A}$ and $\mathbf{B}\delta$, arising from the splitting of a perfect dislocation of Burgers vector **BA** on the d plane.

tacts were made by gently forcing the tip to progress towards the sample once the tunneling current had been established.

We report the characterization of two different types of defects. A representative example of the first one, which we call type I, is shown in Fig. 2(a). At this amplification, the moiré pattern originated from the superposition of the hexagonal overlayer on the square substrate (the $5\times n$ reconstruction) is discernible as quasi-one-dimensional ridges running along [110]. The type-I defect is viewed as a line from point M to N that interrupts the ridges and causes a phase shift. From images of different type-I defects, we estimate the length of the line joining the M and N points as $l=72\pm15$ Å, with the uncertainty deriving mainly from the moiré broadening. The height of the step, estimated from profiles like the one represented in Fig. 2(b) is $s=0.65\pm0.10$ Å. The second type of defect (type II) is shown in Fig. 3(a): it can be described as an elevated tableland with a mean height of 0.75 ± 0.10 Å. It rises abruptly when either the MN or $M'N'$ line is crossed and descends gently, and *asymmetrically*, in the perpendicular direction [see profiles in Fig. 3(b)].

Although mobile vacancy clusters, one atomic plane deep (≈2 Å in Au), have been earlier described around STM nanoindentations,[14] our type-I and -II defects have a very different morphology. We relate them to dislocations on the basis of microindentation tests, in which dislocations are known to generate and propagate from the contact point of the indentor (current work[15] is extending this idea to nanocontacts). Around these contact points, dislocation loops with Burgers vectors **b** *parallel to the surface* tend to prevail.[7] If **b** has a component perpendicular to the surface ($\mathbf{b}\cdot\mathbf{n}\neq0$, **n** being the normal), dislocations in STM pictures are recognized through the observation of their associated steps. If **b** is parallel to the surface, dislocations can be imaged only through the influence of their displacement fields on the neighboring atoms. We have developed a model[16] that includes a number of assumptions, namely, (i) sample atoms are represented by hard spheres on the grounds of atomic-charge superposition.[12] (ii) The 5×23 reconstruction is introduced by constructing a gold hexagonal compact layer with a uniform contraction of 4%,[13] and letting that layer descend onto the Au(001) unreconstructed substrate until every atom in the hexagonal layer contacts the underlying first unreconstructed plane. In the latter, the actual position of the atoms around a dislocation are computed by the well-known formulas of standard dislocation theory.[7] The z position of every atom in the uppermost hexagonal layer is then taken as the final surface configuration, without allowing for lateral displacements. The reconstructed layer is, then, completely uncoupled to the rest of the crystal. Theoretical support for the floating nature of the hexagonal overlayer in Au(100) is discussed by Fiorentini, Methfessel, and Scheffler[17] and the assumption is further supported by x-ray diffraction data[18] that show that, in spite of the different substrates, the recon-

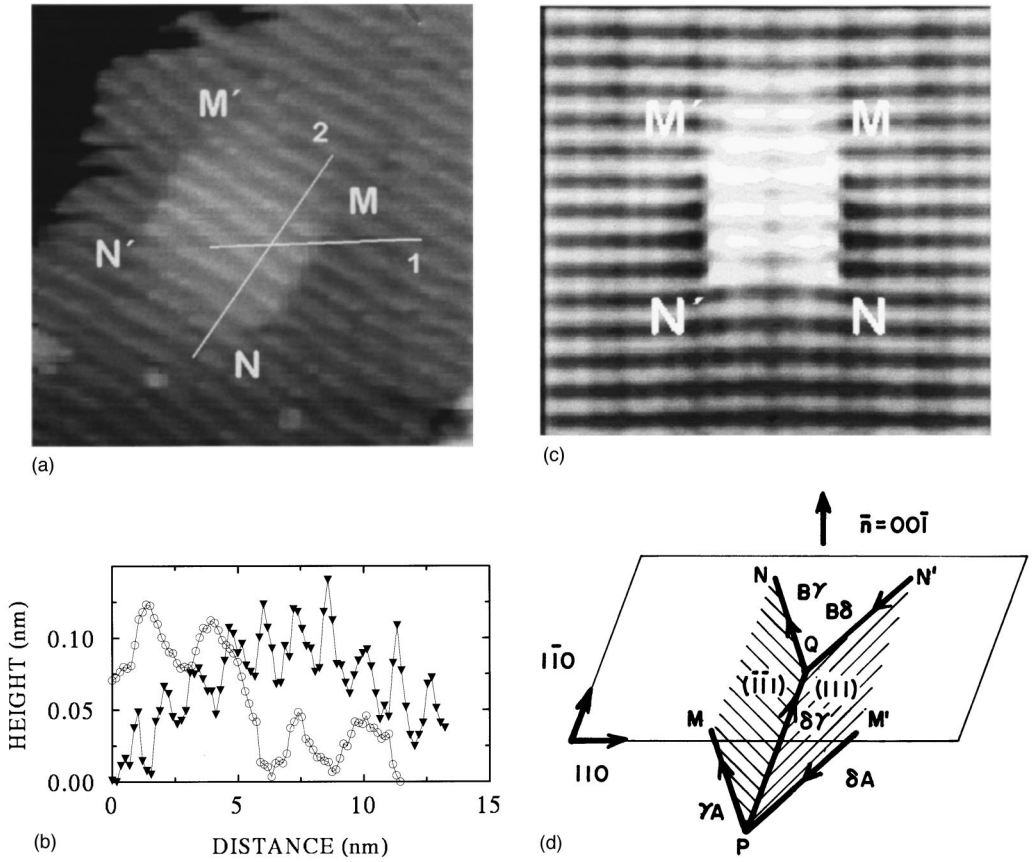

FIG. 3. (a) STM image of a type-II defect (dissociated perfect dislocation loop), showing two opposite steps perpendicular to the reconstruction direction. The size of the image is 240×240 Å. (b) Profiles along the solid lines 1 (○) and 2 (▼) of the image (a). (c) Simulated image of the dislocation configuration described in (d). (d) Dislocation configuration of a defect type II: Double splitting of the initial loop gives rise to four Shockley partials whose emergency points correspond to the M, N, M', and N' points and to a stair rod along PQ. All Burgers vectors are shown in the scheme.

structed overlayer is the same in Au(100) and Au(111). (iii) In order to describe the atom displacements around the proposed dislocation configuration, the displacement fields of *infinite* dislocations have been used. The effect of considering finite dislocation segments will be analyzed elsewhere.[16] A gray-level scale was used to convert the simulation data into images, which were finally sent through a Fourier low-pass filter in order to simulate the effective resolution of the experimental image.

As is well known from standard dislocation theory, in *bulk* fcc metals perfect dislocations of Burgers vector $a/2\ \langle 110\rangle$, a being the cube side, tend to split into two Shockley dislocations of Burgers vector $a/6\ \langle 112\rangle$ that encompass a ribbon of stacking fault.[7] In Fig. 2(c) we represent the simulation, according to the model described above, of the contrast arising from the split dislocation of Fig. 2(d). From the comparison of Figs. 2(a) and 2(c) we propose that the type-I defects are extended dislocations of width l. In particular, the height s of the step associated with the extended dislocation would be given by the scalar product $a/6\,[121]\cdot[001]$ which, for gold, is equal to 0.68 Å, in good agreement with the experimental value of 0.65 Å.

We argue now that type-II defects are split loops whose geometry is represented in Fig. 3(d). We employ the standard Thomson's tetrahedron notation.[7] Let us assume that the loop is V shaped (intersecting the surface) with segments MPM' along **DB** and **BC**, and Burgers vector **BA**, in Thomson's notation. Once the loop is extended, the segment along **DB** splits across the c plane into two parallel Shockley partial dislocations with Burgers vectors $\gamma\mathbf{A}$ and $\mathbf{B}\gamma$. In the same way, the segment along **BC** splits in the d plane into two parallel Shockleys with Burgers vectors $\delta\mathbf{A}$ and $\mathbf{B}\delta$. As a result of the double splitting, a segment of stair-rod dislocation along **BA**, with Burgers vector $\delta\gamma$ is originated. The result of the simulation is shown in Fig. 3(c). An *asymmetric* tableland of mean height ≈ 0.7 Å is obtained, with phase shifts appearing when the stacking-fault ribbons traces (MN or $M'N'$) are crossed. There is remarkable agreement between this simulation and the STM image and profile [Figs. 3(a) and 3(b)], including the profile asymmetry along the [110] direction. If, maintaining the Burgers-vector values, the dislocation orientations are taken instead along $\mathbf{D}\gamma$ and $\mathbf{C}\delta$, no profile asymmetry along this direction results. We take it as evidence of the proposed assignment (**DB** and **BC**) of the dislocation directions.

A simple geometrical construction shows that if α is the angle between the dislocation direction (NQ) and the stacking-fault trace (NM)—see Fig. 3(d)—then the relationship between the experimental length l and the width R of the extended dislocation is $R=l\ \sin\alpha$. For partials along **DB** $\alpha=\pi/6$, $R=l\sqrt{3/2}=62$ Å. This is definitely larger than the split observed in the bulk,[19] 40 Å, for the same angle of $\pi/6$

between the dislocation line and the Burgers vector of the undissociated dislocation. Whereas introducing the role of surfaces on the dislocation interaction,[20] and allowing for finite segments, could result in changes in the equilibrium width of the stacking-fault ribbon,[16] within the present understanding, the possibility that the stacking-fault energy is altered near the surface cannot be discarded. One can think of the split as a testing ground for the interaction of dislocations with surfaces. It is worth remarking that split dislocation loops can provide an efficient path to strain relief in metal surfaces with square symmetry, akin to the internal (111) faceting reported for Cu/Ni(100).[21]

Using a time-honored procedure in TEM,[7,8] the observed splitting of partial dislocations in Figs. 2 and 3 can be used to derive a stacking-fault energy density γ by equating the elastic dislocation repulsion per unit length F_{L} to $-\partial W_{\mathrm{SF}}/\partial R$, W_{SF} being the energy per unit length of the stacking-fault ribbon. Using isotropic elastic continuum theory, one obtains[7]

$$\gamma = F_L = (\mu/2\pi R)\{(\mathbf{b}_1\cdot\xi)(\mathbf{b}_2\cdot\xi) + (1-\nu)^{-1}(\mathbf{b}_1\times\xi)\cdot(\mathbf{b}_2\times\xi)\}, \quad (1)$$

where **b** stands for the Burgers vector, ξ for the dislocation direction unit vector, R for the distance between the partials, and μ and ν are the Voigt elastic parameters of Au.[7]

Using our experimental value $R=62$ Å we obtain $\gamma=19\pm5$ ergs cm^{-2}. If anisotropy is introduced, using the Jenkins calculations[19] instead of Eq. (1), the value $\gamma=18\pm$ ergs cm^{-2} is obtained. Indeed, the use of an elastic continuum involves a number of approximations; inclusion of additional terms (as computed from molecular dynamics) tends to increase the expected split for a given γ. However, the correction is not very large[22] and unlikely to explain why our γ values fall outside the accepted range in the bulk.[23]

In summary, we have shown that STM dislocation images can be interpreted in terms of a simple model. Although other groups have reported the observation of splitting into partials of perfect dislocation lines, using this technique, here dislocation *directions* and Burgers vectors are assigned on the basis of calculation involving the dislocations' displacement field. In the neighborhood of contact of an STM tip with a Au(001) crystal surface, we have also observed configurations of extended dislocations, particularly the splitting of an unfaulted dislocation *loop* with Burgers vector parallel to the surface; the resulting configuration consists of four segments of Shockley partial dislocations connected by a stair-rod dislocation parallel to the surface. The width of the extended dislocations seems rather sensitive to surface proximity, being significantly larger than in the bulk. It is hoped that this work will open the way to a systematic analysis of dislocation configurations near the surface and of the actual role of the surface on the onset of glide systems around nanoindentation contacts.

Part of this work has been financed by the Spanish CICyT through Project No. PB94-1527. Useful discussions with C. B. Carter are acknowledged.

[1] W. K. Burton, *et al.*, Philos. Trans. R. Soc. London, Ser. A **243**, 299 (1951).
[2] R. Beanland *et al.*, Adv. Phys. **45**, 87 (1996).
[3] G. A. Somorjai, *Surface Chemistry and Catalysis* (Wiley, New York, 1996).
[4] J. C. Hamilton and S. M. Foiles, Phys. Rev. Lett. **74**, 2760 (1995).
[5] R. Q. Hwang *et al.*, Phys. Rev. Lett. **75**, 4242 (1995); R. Q. Hwang and C. B. Carter, Phys. Rev. B **51**, 4730 (1995).
[6] S. J. Basinski and Z. S. Basinski, in *Dislocations in Solids*, edited by F. R. N. Nabarro (North-Holland, Amsterdam, 1979), Vol. 4, pp. 270–286.
[7] J. P. Hirth and J. Lothe, *Theory of Dislocations*, 2nd ed. (McGraw-Hill, New York, 1972); F. R. N. Nabarro, *Theory of Crystal Dislocations* (Dover, New York, 1987).
[8] P. B. Hirsch *et al.*, *Electron Microscopy of Thin Crystals* (Butterworths, London, 1965).
[9] A. Samsavar *et al.*, Phys. Rev. Lett. **65**, 1607 (1990); J. F. Wolf and H. Ibach, Appl. Phys. A: Solids Surf. **52**, 218 (1991); J. Jacobsen *et al.*, Phys. Rev. Lett. **75**, 489 (1995).
[10] G. Cox *et al.*, Phys. Rev. Lett. **64**, 2402 (1990); M. Schmid *et al.*, *ibid.* **69**, 925 (1992); Z. Gai, Y. He, X. Li, J. F. Jia, and W. S. Yang, Surf. Sci. **365**, 96 (1996).
[11] M. Ghaly and R. Averback, Phys. Rev. Lett. **72**, 364 (1994).
[12] J. Tersoff and D. R. Haman, Phys. Rev. B **31**, 805 (1985).
[13] G. Binnig *et al.*, Surf. Sci. **144**, 321 (1984).
[14] J. de la Figuera *et al.*, Solid State Commun. **89**, 815 (1994).
[15] C. L. Kelchner and J. C. Hamilton (private communication).
[16] M. A. González *et al.*, (unpublished).
[17] V. Fiorentini *et al.*, Phys. Rev. Lett. **71**, 1051 (1993).
[18] S. G. J. Mochrie *et al.*, Phys. Rev. Lett. **64**, 2925 (1990).
[19] M. L. Jenkins, Philos. Mag. **26**, 747 (1972).
[20] P. M. Hazzledine *et al.*, Philos. Mag. **32**, 81 (1975).
[21] B. Müller *et al.*, Phys. Rev. Lett. **76**, 2358 (1996).
[22] J. Boehm and R. M. Nieminen, Phys. Rev. B **53**, 8956 (1996).
[23] An earlier compilation by P. C. J. Gallagher, Metall. Trans. A **1**, 2429 (1970), which is still widely used, recommends $\gamma=30-40$ ergs cm^{-2}. More recently, Jenkins (Ref. 19), using the weak-beam technique, obtained a value of $\gamma=32\pm5$ ergs cm^2.